
A Generic Machine Learning Framework for Radio Frequency Fingerprinting

Alex Hiles and Bashar I. Ahmad

Applied Intelligence Labs, ITG, Defence

Digital Intelligence, BAE Systems, Chelmsford, Essex, CM2 8HN

Abstract

Fingerprinting Radio Frequency (RF) emitters typically involves finding unique emitter characteristics that are featured in their transmitted signals. These fingerprints are nuanced but sufficiently detailed, motivating the pursuit of methods that can successfully extract them. The most granular downstream task is known as Specific Emitter Identification (SEI), which requires a well informed RF fingerprinting (RFF) approach for it to be successful. RFF and SEI have a long history, with numerous application areas in defence and civilian contexts such as signal intelligence, electronic surveillance, physical-layer authentication of wireless communication devices, to name a few. RFF methods also support many other downstream tasks such as Emitter Data Association (EDA) and RF Emitter Clustering (RFEC) and are applicable to a range of transmission types. In recent years, data-driven approaches have become popular in the RFF domain due to their ability to automatically learn intricate fingerprints from raw data. These methods generally deliver superior performance when compared to traditional techniques. The more traditional approaches are often labour-intensive, inflexible and only applicable to a particular emitter type or transmission scheme. Therefore, we consider data-driven Machine Learning (ML)-enabled RFF. In particular, we propose a generic framework for ML-enabled RFF which is inclusive of several popular downstream tasks such as SEI, EDA and RFEC. Each task is formulated as a RF fingerprint-dependent task within the framework. A variety of use cases using real RF datasets are presented here to demonstrate the framework for a range of tasks and application areas, such as spaceborne surveillance, signal intelligence and countering drones.

1. Introduction

RFF involves building emitter representations from characteristics that are present in their signals. This can be particularly useful for downstream tasks such as SEI, which involves classifying signals into their emitter origination (e.g. differentiating between various radars, 5G sources, etc) [21; 44]. In general, the emitter characteristics are unintentional (e.g., the waveform, transmission timing or bandwidth), caused by the channel (e.g., Doppler frequency offset, dispersion, scintillation), or intentional [21]. Intentional characteristics are often assumed to originate from inherent transmitter hardware imperfections (e.g., amplitude rise-time, ripple, phase distortion, nonlinearities in the transmitter processing chain, antenna responses) and/or are induced by manufacturing variabilities, including individual components in the transmitter processing chain. Spoofing or concealing these characteristics is difficult, allowing tasks such as SEI to be possible. Overall, RFF involves finding set of specific characteristics or features (intentional or not) which are unique to a RF emitter that can be extracted from the received transmission [21; 44].

In practice, datasets containing received transmissions are collected, and subsequently used by a RFF approach in order to extract emitter characteristics. These datasets also contain different types of transmissions or modulation schemes, allowing us to solve other less relevant identification tasks such as distinguishing between types of transmissions or types of modulation. The primary goal here, however, is to obtain RF fingerprint representations which allow us to solve tasks such as SEI, since solving this task requires a detailed account of the intentional features originating from the emitters' hardware imperfections. More generally, emitter classification can be on the individual hardware unit level (e.g. SEI) or even coarser (e.g. individual manufacturers). Consequently, RFF for SEI is the most detailed and nuanced, typically exploiting unintentional features originating from the emitters' hardware imperfections and/or manufacturing variabilities to solve the SEI task successfully. Note that broader emitter class characteristics such as type, modulation scheme, central frequency, used waveform, etc may also be used either implicitly or explicitly to inform RFF.

A Generic Machine Learning Framework for Radio Frequency Fingerprinting

In general, there are two different ways to approach RFF:

1. Traditional RFF with signal processing techniques [4; 8; 9; 13; 19; 25],
2. Deep Learning (DL)-based, ML, RFF [15; 42; 45; 47; 50].

The first approach manually defines unique features/characteristics that form the RF fingerprint for a sought set of emitters (e.g., evolution of the signal’s frequency spectrum or its amplitude envelope). Subsequently, a suitable conventional signal processing (SP) algorithm is then applied to extract this RF fingerprint. In general, such conventional approaches to RFF can be effective and their outputs fully explainable. However, these techniques are inherently inflexible and are usually specific to a particular type of emitter/signal or classification requirement. In addition, they require considerable effort by specialists for each application or emitter/signal type. For example, they may need to manually define the new RF fingerprint and devise or adapt the associated SP method. This renders their development cycle for new types or classes of emitters slow, labour-intensive and expensive. This is particularly problematic in the increasingly congested and contested electromagnetic environment (EME), where new emitters emerge regularly and communication technologies continuously evolve. Therefore, a more versatile and flexible approach to RFF might be required.

The second approach is to use data-driven techniques, which typically leverage (state-of-the-art) SOTA ML model architectures, to address RFF. In the RFF domain, these methods typically employ deep neural networks to extract salient features of individual emitters from the input data, performing automatic RFF whilst simultaneously carrying out a downstream task such as SEI [11]. These DL models have emerged in recent years and have been widely observed delivering superior performance when compared with more traditional methods. Across different types of emitters and signals, these DL approaches are more adaptable for tasks such as signal/modulation-scheme classification, SEI, anomaly detection, amongst others, and have robustness to adverse conditions (e.g. propagation channel and interference) when compared with conventional SP-based approaches [21].

ML, more so DL-based, RFF has the following advantages when compared to conventional SP approaches: (1) It automatically learns nuanced RF fingerprints directly from received transmissions (e.g., from In-phase/Quadrature (I/Q) data streams) whilst simultaneously performing one or more of several possible downstream problems, such as SEI. If SEI is applied, then larger emitter classes can be easily and naturally derived from the detailed RFFs. This

circumvents the labour-intensive step of pre-defining them and devising bespoke algorithms to extract them. (2) It enables generic and flexible, multi-purpose, RFF and downstream tasking (RFF-DT), such as SEI, that can be applied to various emitters and signal types including new, previously unseen emitters (with a suitably developed end-to-end ML pipeline). For example, the SEI model can be re-trained/adapted considering the available data from the previously unseen emitters. ML-based RFF-DT, therefore, not only offers a faster development and iterative testing-refinement cycle, but also superior performance (e.g. more accurate identification), including at lower Signal-to-Noise Ratio (SNR) levels. It is emphasised that ML-based RFF strictly refers to automatically extracting the latent RF fingerprint from the input data. This is fundamentally distinct from methods that only apply a ML classifier to an extracted set of features from the received signal (e.g. emitter/signal identification).

The above benefits of ML-based approaches come at the cost of needing to have data (RF captures), with a certain level of data labelling [22; 65], pertaining to the targeted emitters. The quantity of data can also vary depending on the application, but few-shot methods [59] can address this problem should large quantities of data be available for similar types of emitters to those under investigation. In addition to this problem, it is not always guaranteed that the trained model has captured the correct features despite being successful at the task it has been trained to do. For example, the model could latch onto noise profiles in the data which allow it to be successful at the task. Therefore, it is important to ensure that appropriate guardrails are put in place so that this scenario is mitigated.

A block diagram of ML-based RFF-DT is depicted in Figure 1. The block diagram shows the representation learning

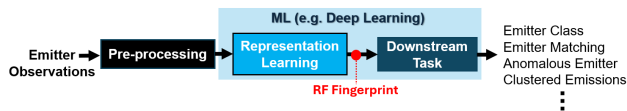


Figure 1. Block diagram of ML-based RFF-DT.

module before the downstream task, which is where RF fingerprints are learnt directly from the input data. These fingerprints can have different “levels of supervisions”, referring to the relationship of the RF fingerprint representation learning block and the downstream task block. Most importantly, a general model can be learnt for RFF across numerous emitters or conditions, which can then be adapted or fine-tuned to a specific set of emitters or conditions. The downstream task block can be one or more of the following tasks: (1) Identification of emitters, inclusive of SEI; (2) Comparing and matching multiple emitter emissions originating from the same emitter (e.g. EDA, typically solved

using contrastive learning [7]); (3) Automatic grouping and building of RF fingerprint libraries for unknown emitters [27; 53]; (4) Anomaly detection based on learning RFF “normalcy” models, or a generative approach (e.g. variational auto encoders (VAEs)) for detecting and spoofing [70]; (5) Authentication (physical-layer) by comparing RF fingerprints to received signals [37]. In this paper, the ML-based RFF problem is mathematically framed. The main contributions in this paper are as follows:

1. A generic framework for ML-based RFF is introduced, providing a basis for treating existing or future novel RFF-related downstream tasks.
2. Individual RFF downstream tasks are formulated within the presented framework and solved using a variety of real world datasets, including Automatic Identification System (AIS) data from spaceborne receivers, Digital Mobile Radio (DMR) data and drone RF links data.
3. ML-based RFF model performance is demonstrated on real RF data for a variety of tasks and model architectures, spanning across a number of use cases including Spaceborne Intelligence Surveillance and Reconnaissance (ISR), Signals Intelligence (SIGINT) and Counter Unmanned Aerial Systems (C-UAS).
4. Review of existing SOTA RFF ML-based methods, with a focus on input representations, challenges in closed set and open set downstream tasks, as well as mitigations towards the impact of the propagation channel and responses of various receivers.

2. Overview and Related Work

2.1. ML-based RFF approaches

A large corpus of research on ML-based RFF exists in the general wireless communications community, especially for Internet of Things (IoT) and cyber security applications [62]. Various DL models have been adopted and tailored for RFF. For example, convolutional neural networks (CNNs) [66], recurrent neural networks (RNNs) [38], long short-term memory (LSTMs) [50], transformers [55], generative adversarial networks (GANs) [39], auto-encoders (AEs) [67], variational auto-encoders (VAEs) [23], amongst many others have all been applied towards RFF-based problems. CNNs in particular, including complex valued CNNs (CV-CNNs) [24], are amongst the most widely used model architectures. This is generally attributed to their wide availability across different ML libraries/tools and ability to capture temporal correlations in the processed RF signals.

2.2. Closed-set vs Open-set Tasks

The various RFF-based downstream tasks (with the exception of unsupervised learning approaches) can be viewed in terms of being a:

1. **Closed-set Downstream Task (CS-DT)** : constrained to only consider classes that are within a predefined set of emitters, for which there is existing labelled data/recordings;
2. **Open-set Downstream Task (OS-DT)** : new, previously unseen during training, emitters are accounted for. These methods recognise and address them appropriately.

The vast majority of research in ML-based RFF are CS-DT based approaches. For OS-DT, new emitters with respect to a trained CS-DT model need to be identified (e.g. compared to the closed-set members) and their fingerprints learnt such that they can be recognised in a future iteration of the CS-DT model [64]. There are several approaches which have been taken to address this issue, including class incremental learning [27; 28; 30; 71]. These methods can be viewed in the context of anomaly detection for cyber security applications and/or detecting adverse channel conditions.

2.3. Input Representations

Broadly speaking, ML-based RFF-DT methods can be categorised by their input representation:

1. **Time-domain signal**: refers to the received I/Q signals of the detected transmission from the targeted emitter and/or their components from empirical mode decomposition, variational mode decomposition, etc. CNNs and RNNs are a common choice for these types of RFF algorithms, including CV-CNNs and LSTMs. Directly using the I/Q data of the detected transmission is highly desirable for a multi-purpose RFF capability for various emitters and scenarios.
2. **Spectrogram or transform-domain**: bi-spectrum analysis [32] and short-time Fourier Transformer (STFT) [51], Hilbert-Huang [33], and wavelet transforms [63] as well as histograms and grouping input data fall into this category. The resultant representations (or information extracted from them) are then fed into a neural network, often a CNN. Any such transformation should preserve the relevant information in the (complex) time domain RF data to facilitate the superior feature extraction capability of the DL algorithms.
3. **Constellation-based**: relies on the differential constellation trace figure, often based on the modulation

scheme adopted by the emitter [42]. This modality is applicable to communication signals and these constellation traces typically serve as an input to a multi-channel CNN. However, emitter classification from the constructed constellation trace can be challenging in practice and will be specific to an emitter type/modulation scheme, i.e., leads to an inflexible RFF capability.

Time series inputs can include either the transient or the steady-state, or both, components of the received signal. The transient is related to when the transmitter turns on (e.g. beginning of the received burst) and usually incorporates more prominent unique intrinsic distinguishing features originating from hardware imperfections [54]. The steady-state segment often contains the communication content, if relevant, and follows from the transient phase. As well as message-related consistent patterns (e.g. preamble/training-sequence, if relevant), steady-state segments still contain salient transmitter features that can be useful.

2.4. Mitigating Impact of Propagation Channel and Responses of Various Receivers

In practice, the received signal can be substantially impacted by multipath, fading and noise from the propagation channel. Similarly, inherent differences amongst various deployed receivers (e.g. distributed on different satellites in a constellation) can induce a significant mismatch (e.g. distribution shift) between the training dataset and the signals that the ML RFF approach must handle when deployed. Naturally, these scenarios degrade the performance of any RFF-based model. Therefore, successful RFF-based models need to incorporate, where needed, model adaptation, domain adaptation, transfer learning and few-shot learning approaches. All of these approaches enable generalisable and robust ML-based RFF as well as SEI [29; 58; 60; 68]. The aim of these approaches is to improve the resilience of the model in light of certain environmental and sensing conditions. These methods have been tested and applied in numerous research papers on real and synthetic datasets that pertain to complex environments (e.g. dense urban or indoor settings) and for transmission frequencies which are particularly susceptible to channel effects (e.g. deep fading such as with ZigBee [66], Bluetooth low energy [3] and Wi-Fi [17]).

3. Problem Formulation

In this section, we formally introduce the framework for learning general-purpose RF fingerprint representations using ML. Let us assume that we have a dataset $\mathcal{D} = (\mathbf{X}, \mathbf{Y}) \in \mathcal{X} \times \mathcal{Y}$ where \mathbf{X} and \mathbf{Y} are sampled from the

unknown joint probability distribution $\mathcal{P}_{\mathcal{X}\mathcal{Y}}$, where \mathcal{X} is the RF feature space and \mathcal{Y} is the label space. We define a *task* \mathcal{T} to be composed of the dataset \mathcal{D} , a loss function \mathcal{L} and model parameterizations \mathbf{g}_ϕ and \mathbf{F}_θ , where \mathbf{g}_ϕ is the task head, and \mathbf{F}_θ is a vector-valued RFF function that contains, or is equivalent to, the RF fingerprint head $\mathbf{f}_\theta : \mathcal{X} \mapsto \mathcal{Z}$, where \mathcal{Z} is the RFF representation space. In general, $\mathbf{F}_\theta : \mathcal{X} \times \dots \times \mathcal{X} \mapsto [\mathcal{Z}]^l$, where l denotes the number of RF fingerprint head projections that have been made and $[\mathcal{Z}]^l \triangleq \mathbb{R}^{d \times l}$. For the majority of tasks, such as SEI, $l = 1$ and the vector-valued function $\mathbf{F}_\theta \equiv \mathbf{f}_\theta$ whereas for other tasks, such as EDA, $l > 1$.

The composite function $\mathbf{h}_\xi(\mathbf{x}) \triangleq \mathbf{g}_\phi(\mathbf{F}_\theta(\mathbf{x}))$ projects the input data $\mathbf{x} \in \mathbf{X}$ to a prediction $\hat{\mathbf{y}}$, which is computed for every $\mathbf{x} \in \mathbf{X}$, forming a predictive labels set $\hat{\mathbf{Y}} = \{\hat{\mathbf{y}} | \hat{\mathbf{y}} = \mathbf{h}_\xi(\mathbf{x}), \mathbf{x} \in \mathbf{X}\}$. The loss function \mathcal{L} measures the distance between any pairs of $(\mathbf{y}, \hat{\mathbf{y}}) \in \mathbf{Y} \times \hat{\mathbf{Y}}$ and is used to supervise model training, and $\mathbf{g}_\phi : [\mathcal{Z}]^l \mapsto \mathcal{Y}$ is a mapping from $[\mathcal{Z}]^l$ to the label space \mathcal{Y} .

Notationally, we represent the k th *task* with superscripts (e.g. t th task dataset $\mathcal{D}^{(t)}$), where each task is assumed to be sampled from the probability distribution of tasks $\mathcal{P}_{\mathcal{T}}$ and $\mathcal{D}^{(t)} = (\mathbf{X}^{(t)}, \mathbf{Y}^{(t)}) = \{(\mathbf{x}_i^{(t)}, y_i^{(t)})\}_{i=1}^{n_t} \sim \mathcal{P}_{\mathcal{X}^{(t)}\mathcal{Y}^{(t)}}$. Therefore, we also have the t th task predictive labels set $\hat{\mathbf{Y}}^{(t)}$. Note that for some tasks, the parameter set ϕ is fixed since the function \mathbf{g} is a deterministic function (e.g. distance measure) but for others is learnable. For example, \mathbf{g}_ϕ maps the lower-dimensional representation to the classification label space for a SEI task, whereas for an EDA task, \mathbf{g}_ϕ is a distance measure (e.g. cosine distance) between two RF input embeddings. Hence, ϕ is not strictly learnable whereas θ is.

3.1. Multi Task RF Fingerprint Learning

We first introduce the following optimization problem:

$$\min_{\xi \in \Xi} \mathbb{E}_{t \sim \mathcal{P}_{\mathcal{T}}} \left[\mathbb{E}_{\mathcal{D}^{(t)} \sim \mathcal{P}_{\mathcal{X}^{(t)}\mathcal{Y}^{(t)}}} \mathcal{L}^{(t)} \left(\mathbf{h}_{\xi_t}^{J, (t)} \left(\mathbf{X}^{(t)} \right), \mathbf{Y}^{(t)} \right) \right],$$

where $\mathbf{h}_{\xi_t}^{J, (t)}(\mathbf{X}^{(t)}) = \mathbf{g}_{\phi_t}^{(t)}(\mathbf{F}_\theta^{(t)}(\mathbf{X}^{(t)}))$, with superscript J representing that θ is jointly learnt across tasks, $\Xi = \Theta \times \Phi$, $\Theta \equiv \mathbb{R}^d, d \in \mathbb{Z}^+$, $\Phi = \Phi_1 \times \dots \times \Phi_{|\mathcal{P}_{\mathcal{T}}|}$, $\Phi_j \equiv \mathbb{R}^{c_j}, c_j \in \mathbb{Z}^+$, with $\theta^* \in \Theta$, $\phi^* = (\phi_1^*, \dots, \phi_{|\mathcal{P}_{\mathcal{T}}|}^*)$ with $\phi_j^* \in \Phi_j \forall j \in \{1, \dots, |\mathcal{P}_{\mathcal{T}}|\}$. Upon solving the above optimization task, we jointly learn the RF fingerprint parameters θ and the task-specific parameter sets ϕ_t , for all t .

We define the parameters ξ^* as an argument minimizer of the optimization problem above. Intuitively speaking, it is expected that the resulting RF fingerprint head \mathbf{f}_{θ^*} has an increasingly richer RFF representation when jointly learning θ across an increasing amount of tasks that require RF fin-

gerprint knowledge. It is assumed that the functional form of the RF fingerprint head is chosen to be the same across all tasks. In other words, $\mathbf{F}_\theta^{(t)} = \mathbf{F}_\theta$ where \mathbf{F}_θ is chosen appropriately.

Alternatively, we can learn across all tasks but have independent parameter sets θ_t for each task t and aggregate them post optimization. Mathematically speaking,

$$\min_{\xi \in \Xi} \mathbb{E}_{t \sim \mathcal{P}_T} \left[\mathbb{E}_{\mathcal{D}^{(t)} \sim \mathcal{P}_{\mathcal{X}^{(t)}\mathcal{Y}^{(t)}}} \mathcal{L}^{(t)} \left(\mathbf{h}_{\xi_t}^{I,(t)}(\mathbf{X}^{(t)}), \mathbf{Y}^{(t)} \right) \right],$$

where $\mathbf{h}_{\xi_t}^{I,(t)}(\mathbf{X}^{(t)}) = \mathbf{g}_{\phi_t}^{(t)} \left(\mathbf{F}_{\theta_t}^{(t)}(\mathbf{X}^{(t)}) \right)$, with I denoting that an independent parameter set θ_t is being learnt for each task. An aggregation function $a : \Theta_1 \times \dots \times \Theta_{|\mathcal{P}_T|} \mapsto \mathbb{R}^d$ can then be used to combine the parameters into one parameter set θ^* . In other words, $\theta^* = a(\boldsymbol{\theta}^*)$. One possible composition of the aggregation function a could be $a(\mathbf{x}) = \frac{1}{n} \sum_{i=1}^n x_i$, for example.

In the discrete setting, we assume that m tasks exists, where the t th task has a dataset $\mathcal{D}^{(t)}$, with each data point $\mathbf{z} \in \mathcal{D}^{(t)}$ being Independent Identically Distributed (IID) and assumed to be drawn from an unknown joint probability distribution $\mathcal{P}_{\mathcal{X}^{(t)}\mathcal{Y}^{(t)}}$. This results in the following optimization problems:

$$\boldsymbol{\xi}_{S,J}^* = \arg \min_{\xi \in \Xi} \sum_{t=1}^m \frac{\alpha_t}{n_t} \sum_{j=1}^{n_t} \mathcal{L}^{(t)} \left(\mathbf{h}_{\xi_t}^{J,(t)}(\mathbf{x}_j^{(t)}), \mathbf{y}_j^{(t)} \right),$$

$$\boldsymbol{\xi}_{S,I}^* = \arg \min_{\xi \in \Xi} \sum_{t=1}^m \frac{\alpha_t}{n_t} \sum_{j=1}^{n_t} \mathcal{L}^{(t)} \left(\mathbf{h}_{\xi_t}^{I,(t)}(\mathbf{x}_j^{(t)}), \mathbf{y}_j^{(t)} \right),$$

where the argument minimizers $\boldsymbol{\xi}_{S,J}^* = (\phi_{S,J}^*, \theta_{S,J}^*) = (\phi_1^*, \dots, \phi_n^*, \theta^*)$ and $\boldsymbol{\xi}_{S,I}^* = (\phi_{S,I}^*, \theta_{S,I}^*) = (\phi_1^*, \dots, \phi_m^*, \theta_1^*, \dots, \theta_m^*)$ for the joint and individual (parameter set for each task) optimization tasks respectively, and α_t denotes the weighting of the t th task with $\sum_{t=1}^n \alpha_t = 1$. A standard choice for this is equal weighting across tasks (e.g. $\alpha_t = 1/n$ for all t), though this formulation allows for this to be selected according to preference. In the same manner as previously discussed, we can aggregate to find $\theta^* = a(\boldsymbol{\theta}^*) = a(\theta_1^*, \dots, \theta_m^*)$.

The resulting parameters found from solving either of these optimization problems are a function of the RFF-based tasks, data quality, loss function and model architecture. In practice, whilst \mathcal{P}_T is unknown, it is assumed that common tasks such as SEI, EDA, RF Emitter Clustering (RFEC), amongst others are the modes of this distribution and approximate the expectation appropriately. Therefore, it is likely that approximate solutions to this optimization problem can be found by jointly considering many popular RF fingerprint-based tasks.

The joint optimization problems introduced here are analogous to multi-modal joint embedding learning techniques

[2; 43; 57], though here the intuition is on solving different tasks in the multi-task learning (MTL) sense [5; 49; 69], rather than enriching the RF representation via multi-modal data. Both formulations are multi-objective optimization problems that serve multi-task learning [49] and are a generic approach towards learning RF fingerprint representation spaces via data-driven methods.

4. Single Task RF Fingerprint Learning

In this section, we provide descriptions of popular RF fingerprint-based tasks using the framework introduced in Section 3. It is noted that only one RFF-based task is considered at a time.

4.1. Closed Set Specific Emitter Identification

The first task we define is closed set SEI (CS-SEI). In this task, the objective is to learn an accurate mapping from emitter observations (typically I/Q samples) to the correct emitter label. Assuming that $\mathcal{P}_{\mathcal{X}^{(i)}\mathcal{Y}^{(i)}}$ is the joint probability distribution of the SEI feature space $\mathcal{X}^{(i)}$ and the emitter label space $\mathcal{Y}^{(i)}$, where the superscript i denotes identification task, we pose the following optimization problem to learn a mapping \mathbf{h}_ξ from $\mathcal{X}^{(i)}$ to $\mathcal{Y}^{(i)}$:

$$\xi^* = \arg \min_{\xi \in \Xi} \mathbb{E}_{(\mathbf{x},y) \sim \mathcal{P}_{\mathcal{X}^{(i)}\mathcal{Y}^{(i)}}} \mathcal{L}^{(i)} \left(\mathbf{h}_\xi^{(i)}(\mathbf{x}), y \right).$$

This translates as finding a suitable parameter set pair $\xi^* = (\phi^*, \theta^*)$ such that $\mathbf{h}_{\xi^*}(\mathbf{x}) = \mathbf{g}_{\phi^*}(\mathbf{F}_{\theta^*}(\mathbf{x})) \approx y \forall (\mathbf{x}, y) \in \mathcal{X}^{(i)} \times \mathcal{Y}^{(i)}$, noting here that for CS-SEI $\mathbf{F}_{\theta^*} \equiv \mathbf{f}_{\theta^*}$.

Since the joint probability distribution is unknown, we cannot solve this optimization problem in its exact form. Instead, we minimize the empirical error, replacing the joint distribution with the sampled empirical data. We assume a dataset $\mathcal{D}^{(i)} = (\mathbf{X}^{(i)}, \mathbf{Y}^{(i)})$ is sampled from $\mathcal{P}_{\mathcal{X}^{(i)}\mathcal{Y}^{(i)}}$, which we expand as $\mathcal{D}^{(i)} = \{(\mathbf{x}_k^{(i)}, y_k^{(i)})\}_{k=1}^{n_i}$ where $\mathbf{x}_k^{(i)} \in \mathbb{R}^{d^{(i)}}$, $y_k \in \{1, 2, \dots, \mathcal{V}\}$, n_i is the number of samples for the identification task and \mathcal{V} is the number of unique emitters. We assume that each data point $\mathbf{z} = (\mathbf{x}, y) \in \mathcal{D}^{(i)}$ is sampled IID from $\mathcal{P}_{\mathcal{X}^{(i)}\mathcal{Y}^{(i)}}$. Then, the CS-SEI optimization problem is defined as:

$$\xi_{em}^* = \arg \min_{\xi \in \Xi} \mathbb{E}_{(\mathbf{x},y) \sim \mathcal{D}^{(i)}} \mathcal{L}^{(i)} \left(\mathbf{h}_\xi^{(i)}(\mathbf{x}), y \right),$$

where the subscript em denotes empirical.

4.2. RFF-based Emitter Data Association

The objective in this task is to learn a model that can determine whether a pair of emitter observations originate from the same emitter or not. In other words, we are interested in finding a function $\mathbf{h}_\xi : \mathcal{X}^{(a)} \mapsto \mathcal{Y}^{(a)} = \{0, 1\}$, where $\mathcal{X}^{(a)}$ is the EDA feature space, and labels 0 and 1 denotes

no match and match respectively. In this case, the model prediction $\hat{y} = \mathbf{h}_\xi^{(a)}(\mathbf{x})$ is parameterized as follows:

$$\mathbf{h}_\xi^{(a)}(\mathbf{x}) = \mathbf{g}_\phi^{(a)}\left(\mathbf{F}_\theta^{(a)}(\mathbf{x})\right) = \mathbf{g}_\phi^{(a)}\left(\mathbf{f}_\theta^{(a)}(\mathbf{x}_1), \mathbf{f}_\theta^{(a)}(\mathbf{x}_2)\right),$$

where $\mathbf{g}_\phi^{(a)}$ for this task is a distance metric (e.g. Euclidean, cosine distance, etc), $\mathbf{F}_\theta^{(a)}$ is a RFF function containing two separate projections of emitter data using the underlying RF fingerprint head $\mathbf{f}_\theta^{(a)}$ and $\mathbf{x} = (\mathbf{x}_1, \mathbf{x}_2) \in \mathcal{X}^{(a)} \equiv \mathbb{R}^{d^{(a)}} \times \mathbb{R}^{d^{(a)}}$ where $d^{(a)}$ is the dimensionality of an emitter's feature space for the EDA task. This results in the following optimization problem:

$$\xi^* = \arg \min_{\xi \in \Xi} \mathbb{E}_{(\mathbf{x}, y) \sim \mathcal{P}_{\mathcal{X}^{(a)} \mathcal{Y}^{(a)}}} \mathcal{L}^{(a)}\left(\mathbf{h}_\xi^{(a)}(\mathbf{x}), y\right)$$

where $\mathcal{P}_{\mathcal{X}^{(a)} \mathcal{Y}^{(a)}}$ is the joint probability distribution of the RF feature space $\mathcal{X}^{(a)}$ and the task label space $\mathcal{Y}^{(a)}$ and $\mathcal{L}^{(a)}$ is the loss function for the EDA task.

Like the CS-SEI task, this optimization problem is solved in practice by collecting empirical datasets that are assumed to be sampled from the typically unknown joint probability distribution. Without loss of generality, it is assumed here that an empirical dataset $\mathcal{D}^{(a)}$ is transformed from the CS-SEI dataset $D^{(i)}$. In other words, $\mathcal{D}^{(a)} = \mathcal{M}(\mathcal{D}^{(i)}) = \{(\mathbf{x}_{1,k}^{(a)}, \mathbf{x}_{2,k}^{(a)}, y_k^{(a)})\}_{k=1}^{n_a}$, where n_a is the number of samples in the dataset, \mathcal{M} is a data transform operator such as the one discussed in Appendix A, $y_k^{(a)} \in \{0, 1\}$ and $(\mathbf{x}_{1,k}^{(a)}, \mathbf{x}_{2,k}^{(a)}) \in \mathbf{X}^{(a)} \equiv \mathbb{R}^{d^{(a)}} \times \mathbb{R}^{d^{(a)}}$. This results in the following optimization problem:

$$\begin{aligned} \xi_{em}^* &= \arg \min_{\xi \in \Xi} \mathbb{E}_{(\mathbf{x}_1, \mathbf{x}_2, y) \sim \mathcal{D}^{(a)}} \mathcal{L}^{(a)}(\hat{y}, y); \\ &= \arg \min_{\xi \in \Xi} \frac{1}{n_a} \sum_{k=1}^{n_a} \mathcal{L}^{(a)}(\hat{y}_k, y_k). \end{aligned}$$

In practice, for the data transformation method listed above, n_a is selected according to a sampling strategy because for large n_i the combinatorics become difficult to manage. We also note here that collecting EDA-specific empirical datasets is also possible.

4.3. Unsupervised Approach for RFEC

In this section, we formulate an unsupervised approach within the ML-based RFF framework. Typical methods for learning data structures and hidden patterns without labels are clustering approaches such as DBSCAN [12] or dimensionality reduction techniques (e.g. Principal Component Analysis (PCA) followed by some method of clustering). Here we describe one which uses an auto-encoder approach for RFEC. Autoencoders typically involve projecting the original data into a lower dimensional representation space,

where the encoded data is then fed through a decoder to reconstruct the original input. If the reconstruction error is small, then the encoded representation is assumed to contain important information of the original data. It is a dimensionality reduction technique similar to PCA. In this setting, the optimization problem is:

$$\xi^* = \arg \min_{\xi \in \Xi} \mathbb{E}_{\mathbf{x} \sim \mathcal{P}_{\mathcal{X}^{(r)}}} \mathcal{L}^{(r)}(\hat{\mathbf{x}}, \mathbf{x}),$$

where $\hat{\mathbf{x}} = \mathbf{g}_\phi^{(r)}(\mathbf{F}_\theta^{(r)}(\mathbf{x}))$, $\mathcal{P}_{\mathcal{X}^{(r)}}$ is the probability distribution of the emitter feature space $\mathcal{X}^{(r)}$, $\mathcal{L}^{(r)}$ is the reconstruction loss associated with the auto-encoding approach, $\mathbf{g}_\phi^{(r)}$ in this task is the decoder and $\mathbf{F}_\theta^{(r)} \equiv \mathbf{f}_\theta$ is the projection of the data into the RFF representation space.

In practice, this optimization problem is solved by collecting an empirical dataset that is assumed to be sampled from $\mathcal{P}_{\mathcal{X}^{(r)}}$ IID n_r times, obtaining a dataset $\mathcal{D}^{(r)} = \{(\mathbf{x}_k^{(r)})\}_{k=1}^{n_r}$, where $\mathbf{x}_k^{(r)} \in \mathbf{X}^{(r)}$ with $\mathbf{X}^{(r)}$ being the sample dataset. Then, the optimization problem is:

$$\begin{aligned} \xi_{em}^* &= \arg \min_{\xi \in \Xi} \mathbb{E}_{\mathbf{x} \sim \mathcal{D}^{(r)}} \mathcal{L}^{(r)}(\hat{\mathbf{x}}, \mathbf{x}) \\ &= \arg \min_{\xi \in \Xi} \frac{1}{n_r} \sum_{k=1}^{n_r} \mathcal{L}^{(r)}(\hat{\mathbf{x}}_k, \mathbf{x}_k), \end{aligned}$$

where $\hat{\mathbf{x}}_k = \mathbf{g}_\phi^{(r)}(\mathbf{F}_\theta^{(r)}(\mathbf{x}_k))$.

4.4. Open Set SEI and EDA

A key challenge when solving any of the above tasks is generalization towards emitter data not contained in the training dataset. Open Set Recognition (OSR) methods determine whether a sample belongs to the original training distribution or not. In the CS-SEI regime, a finite number of emitters are assumed in existence and a model is trained to discriminate between them; predicated on the Closed World Assumption (CWA) [14]. From the OSR lens, the key challenge following training in the CS-SEI regime is to determine whether an individual sample presented to the trained model is an observation from a known emitter or an unknown one. The CWA ensures false positives occur on open set data since the model is designed to predict an emitter class from the set of known emitters. In contrast, the key Open Set (OS) challenge in EDA is understanding when the comparator has observed enough emitters in training such that it generalizes well to unknown ones. In other words, EDA learns to compare and is not conditioned on the emitter class. Without loss of generality, we introduce the OSR-SEI problem within the RFF ML framework using some terminology from [56].

Let us assume two sample datasets $(\mathbf{X}_{known}^{(i)}, \mathbf{Y}_{known}^{(i)})$ and $(\mathbf{X}_{unknown}^{(i)}, \mathbf{Y}_{unknown}^{(i)})$ are drawn from the joint probability distribution $\mathcal{P}_{\mathcal{X}^{(i)} \mathcal{Y}^{(i)}}$ such that $\mathbf{Y}_{known}^{(i)} \cap \mathbf{Y}_{unknown}^{(i)} =$

A Generic Machine Learning Framework for Radio Frequency Fingerprinting

\emptyset , denoting $\mathbf{Y}_{known}^{(i)}$ as the label set of known emitters to the CS-SEI model and $\mathbf{Y}_{unknown}^{(i)}$ as the label set of unknown emitters to the CS-SEI model. Then, we define the CS-SEI dataset $\mathcal{D}_c^{(i)} = \{(\mathbf{x}_k^{(i)}, y_k^{(i)})\}_{k=1}^{n_i}$, where $\mathbf{x}_k^{(i)} \in \mathbf{X}_{known}^{(i)}$, $y_k \in \mathbf{Y}_{known}^{(i)}$, and n_i is the total number of samples. In addition, we define a OSR-SEI dataset $\mathcal{D}_o^{(i)} = \{(\mathbf{x}_k^{(i)}, y_k^{(i)})\}_{k=1}^{n_o} \subset (\mathbf{X}_{known}^{(i)} \cup \mathbf{X}_{unknown}^{(i)}) \times (\mathbf{Y}_{known}^{(i)} \cup \mathbf{Y}_{unknown}^{(i)})$ which may or may not contain unknown unique emitters, with n_o being the total number of samples. Then, we combine the two into a dataset $\mathcal{D}^{(osr,i)} = \{\mathcal{D}_c^{(i)}, \mathcal{D}_o^{(i)}\}$.

In the OSR setting, the goal is to simultaneously learn a model capable of solving the CS-SEI problem defined in Section 4.1 as well as produce a score indicating whether a sample belongs to *any* of the known classes. We define a score function $S(x) \in \{0, 1\}$, which indicates whether a sample x belongs to the class of known emitters or the class of unknown emitters (0 indicates x belonging to a known class whereas 1 indicates x belonging to an unknown class). The two most common ways S can be computed are:

1. Jointly learn $S(x)$ by using $\mathcal{D}_c^{(i)}$ for CS-SEI model training and $\mathcal{D}^{(osr,i)} = \{\mathcal{D}_c^{(i)}, \tilde{\mathcal{D}}_o^{(i)}\}$ for binary classification between known and unknown emitters (where $\tilde{\mathcal{D}}_o^{(i)}$ is a proportion of $\mathcal{D}_o^{(i)}$) then evaluate performance on remaining OSR data $\mathcal{D}_o^{(i)} \setminus \tilde{\mathcal{D}}_o^{(i)}$;
2. Conduct CS-SEI model training using $\mathcal{D}_c^{(i)}$ then use rule-based strategies to compute $S(x)$ (e.g. Maximum Softmax Probability (MSP) with threshold [56] [48]) and use $\mathcal{D}_o^{(i)}$ to assess OSR performance.

A hybrid of the above methods can also be applied (e.g. ensemble methods).

Within the generic RFF framework, either of these tasks translate as solving the following optimization problem:

$$\min_{\xi \in \Xi} \mathbb{E}_{(\mathbf{x}, \mathbf{y}) \sim \mathcal{D}^{(osr,i)}} \mathcal{L}^{(osr,i)} \left(\mathbf{h}_{\xi}^{(osr,i)}(\mathbf{x}), \mathbf{y} \right),$$

where $\mathbf{h}_{\xi}^{(osr,i)}(\mathbf{x}) = \mathbf{g}_{\phi}^{(osr,i)} \left(\mathbf{F}_{\theta}^{(osr,i)}(\mathbf{x}) \right)$, $\mathbf{x} = (\mathbf{x}_c, \mathbf{x}_o)$ and $\mathbf{y} = (y_c, y_o)$ with $(\mathbf{x}_c, y_c) \in \mathcal{D}_c^{(i)}$ and $(\mathbf{x}_o, y_o) \in \mathcal{D}_o^{(i)}$. In this case, $\mathbf{g}_{\phi}^{(osr,i)}$ is not only the classifier head but also the open set score computer and $\mathcal{L}^{(osr,i)}$ could be an OSR-specific objective function such as that in [6]. Once a methodology for scoring has been determined and solved, it can then be used to conduct incremental learning [41] [27], perform CS-SEI with quasi-labelling of OSR samples [28], amongst other methods, to address the OS problem. Figure 2 shows an example pipeline for incorporating OS-SEI.

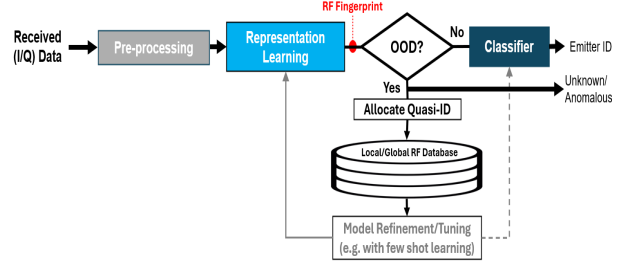


Figure 2. Example pipeline for handling OS-SEI.

5. Experimentation

This section provides a description of real datasets and model architectures used for experimentation as well as documenting experiments which solve a selection of tasks from Section 4.

5.1. Datasets

5.1.1. DIGITAL MOBILE RADIOS: SIGINT

The Digital Mobile Radio (DMR) dataset was collected from eight Commercial Off-The-Shelf (COTS) handsets using a Lime Software Defined Radio (LimeSDR) in four environments; an open field with direct line-of-sight between each DMR and the SDR, two semi-urban environments and one urban environment. The DMR devices are from five different manufacturers, namely one Hytera PD705, one TYT, two Kenwood NX1300D (i.e. identical models), two Entel DX482, and two Motorola DP4400E. All DMRs were programmed to operate in the 433 MHz band where they can use one of the 14 channels, each having a bandwidth of approximately 12.5 kHz. The sampling rate at the receiver was set at approximately 200 kHz. As part of the data pre-processing steps, a burst segmentation algorithm was applied for segments of 30 seconds of continuous transmission to isolate individual bursts from each DMR handset. RFF and identification of individual DMR handsets has several applications in SIGINT and ISR contexts such as determining presence of emitters of interest (e.g. associated with high value targets or threats), tracking them over time and/or building pattern-of-life of their operators.

5.1.2. AIS: SPACEBORNE MARITIME SURVEILLANCE

The Automatic Identification System (AIS) dataset contains transmissions from vessels in the Panama Canal area as captured by SDRs on Low Earth Orbit (LEO) satellites. This proprietary dataset comprises of approximately 10 minutes of RF recording of the VHF channels dedicated to ground maritime AIS emitters. Bespoke pre-processing algorithms are applied to detect-extract the individual AIS bursts and, where possible, demodulate-decode them to obtain their unique Maritime Mobile Service Identity (MMSI)

number, which can serve as a label. It is noted that classical demodulating and decoding techniques for AIS often require relatively high-quality AIS transmissions, for instance a substantially high SNR and/or low levels of interference. The AIS dataset utilised here has over 600 AIS bursts from 48 sources such that each emitter (i.e. with a unique MMSI) has at least 10 transmissions. The sampling rate is approximately 38.4 kHz and the AIS burst time slot is 26.67 m/s.

RFF-based EDA can improve geolocating the transmission source, since by identifying various transmissions that originate from the same source, we can effectively constrain the observables (time and frequency difference of arrival measurements) and dwell on the emitter over a much longer time intervals, thereby utilising multiple emissions in the estimation of the emitters' locations. Whilst geolocation of ground RF emitters from LEO satellite clusters and subsequently tracking changes in their positions (including from multiple passes) has many ISR applications, spaceborne RFF facilitates delivering enhanced situational awareness. For example, results from SEI or EDA can be fused with other data sources, such as images, to confirm identify of vessels and/or detect malicious activities (e.g. spoofing).

5.1.3. DATA FROM DRONES: COUNTER-UAS

RF captures from four identical (i.e. same manufacturer, model and year) small hobbyist drones, Chubory F89, were collected with a COTS SDR in two different settings. These drones use the 2.4 GHz WiFi spectrum for the uplink (controller to drone) and downlink (drone to controller such as video feed) with frequency hopping within. The uplink and downlink transmissions had a central frequency of 2.470GHz, processed bandwidth is approximately 28 MHz to cover several of the subbands (namely, on the uplink transmission) and the SDR sample rate was set at 56MHz. The dataset contains approximately 40,000 emissions per drone. Our objective is to demonstrate that ML-based RFF enables the identification of each individual drone controller from raw I/Q data, in scenarios where the transceivers are the same make and model. This goes well beyond broader classification tasks that might aim to only determine the type of the drone (e.g. based on traditional signal classification) or drone versus non-drone RF emissions. In this context, SEI can facilitate threat detection and inform the patterns of life of drone operators in a C-UAS context. These capabilities can offer a substantial operational advantage in various scenarios, inclusive of cueing C-UAS effectors and resources planning.

5.2. Model Architectures

This section documents model architectures which were used for experimentation. We used architectures that

compose of convolution [26], Long Short Term Memory (LSTM) [18], transformer [55] and fully connected operations. The selection is described below:

1. **Block Convolutional Neural Network (BCNN):** multiple blocks of one-dimensional CNNs, batch normalization [20], leaky rectified linear unit [34] and max pooling layers. Five convolutional blocks are followed by two linear layers with an optional softmax layer;
2. **Bidirectional LSTM (BiLSTM):** a LSTM-based architecture [16]. Here we use the PyTorch implementation with the following parameters: `input_size = 2`, `hidden_size = 512`, `num_layers = 2`, `bidirectional = True`, with a linear layer attached at the end of the model;
3. **GLFormer:** a transformer-based architecture [10] designed for SEI on Spaceborne AIS data. The architecture employs the following mechanisms: sequence embedding, Gated Attention Units (GAUs), Local Self-Attention (LSA), Sliding Local Self-Attention (SLA) [40] and Global Average Pooling (GAP) [31];
4. **VGG19:** one-dimensional variant of VGG19 [52];
5. **Fully Connected Network (FCN):** sequence of linear layers and leaky rectified linear unit activation functions.

For RFEC, we used four different auto-encoder architectures which we named: simpleAE, verysimpleAE, simpleconv1DAE and vanillaAE. The simpleAE architecture is a four layer fully connected network across both the encoder and decoder with leaky ReLU activation after each layer. The verysimpleAE model is the same as simpleAE but with only one layer, simpleconv1DAE parameterizes the encoder with three one-dimensional convolutional layers with batch normalization and leaky ReLU activation followed by three layers of fully connected networks in the encoder and decoder. The vanillaAE architecture is another fully connected network but with three layers in the encoder and decoder as well as batch normalization and leaky ReLU activation.

5.3. Setup

For all three datasets described in Section 5.1, and for all three tasks (SEI, EDA and RFEC), we use raw I/Q as our input representations. We also split each dataset into training, validation and testing datasets. In particular, $\mathcal{D}^{(t)} = \{\mathcal{D}_{train}^{(t)}, \mathcal{D}_{valid}^{(t)}, \mathcal{D}_{test}^{(t)}\}$ where $|\mathcal{D}_{train}^{(t)}| = 1 - p_v - p_t$, $|\mathcal{D}_{valid}^{(t)}| = p_v$ and $|\mathcal{D}_{test}^{(t)}| = p_t$. In our experiments, we choose $p_v = p_t = 0.1$. Across all datasets, we use the

multi-class cross-entropy loss function for SEI, the contrastive loss function for EDA and the mean-squared error loss for RFEC. For a single data sample, these are summarised as:

$$\begin{aligned}\mathcal{L}^{(i)}(\hat{\mathbf{y}}, \mathbf{y}) &= -\sum_{j=1}^{\nu} y_j \log(\hat{y}_j); \\ \mathcal{L}^{(a)}(\hat{y}, y) &= (1 - y) \|\mathbf{f}_\theta(x_1) - \mathbf{f}_\theta(x_2)\|_2^2 \\ &\quad + y \max(0, m - \|\mathbf{f}_\theta(x_1) - \mathbf{f}_\theta(x_2)\|_2^2); \\ \mathcal{L}^{(r)}(\hat{\mathbf{y}}, \mathbf{y}) &= \|\hat{\mathbf{y}} - \mathbf{y}\|_2^2,\end{aligned}$$

where y_j is the ground-truth probability for emitter class j , \hat{y}_j the predicted probability for the j th emitter class, y and \hat{y} in $\mathcal{L}^{(a)}$ are the ground-truth match and predicted match respectively, \mathbf{y} and $\hat{\mathbf{y}}$ are the ground-truth data and encoding of the data vectors in $\mathcal{L}^{(r)}$, m is the margin parameter in the contrastive loss function, and $\|\cdot\|_2$ is the L_2 norm. In order to update the parameters which minimize these loss functions in practice, across the appropriate datasets, we define the iterative parameter update formula:

$$\xi_t^k = \mathcal{U}\left(\tau_k^{(t)}, \mathcal{L}^{(t)}\left(\hat{\mathbf{Y}}_k^{(t)}, \mathbf{Y}^{(t)}\right)\right) \text{ for } k = 1, 2, \dots, K,$$

where $\xi_t^k = (\phi_t^k, \theta_t^k)$, with k referring to the current iteration, t the task, $\tau_k^{(t)}$ the learning rate, $\hat{\mathbf{Y}}_k^{(t)}$ the model prediction, $\mathbf{Y}^{(t)}$ the ground truth label set and $\mathcal{L}^{(t)}$ the loss function. Here, we adopt mini-batch (MB) gradient descent to update the model parameters. Algorithm 1 shows pseudo-code for MB-Single Task Learning (MB-STL), which is executed for each individual task considered here. In our experimentation, we adopt the Adam optimizer method [1] as \mathcal{U} , set the batch size $b_{size} = 512, 128, 128$ for SEI, EDA, and RFEC respectively and assume an epoch k is the completion of $\lceil |\mathcal{D}_{train}|/b \rceil$ batch updates, where $\lceil \cdot \rceil$ is the ceiling function. We choose the number of total epochs to be $E = 200$ unless specified otherwise. Once the model parameter update is calculated via optimizing the loss function, it is mapped into a new parameter update that also minimizes the L_2 norm of the parameters ξ . In PyTorch,

Algorithm 1 MB-STL pseudo-code with stopping criterion

INPUTS: $\mathcal{T} = (\mathcal{D}, \mathbf{g}_\phi, \mathbf{F}_\theta, \mathcal{L}, \mathcal{U})$
INITIALIZE: ξ_0, τ_0
for Epoch $e = 0$ **to** $E - 1$ **do**
 for batch $b = 0$ **to** $B - 1$ **do**
 $\hat{\mathbf{y}}_{e,b} = \mathbf{h}_{\xi_{e,b}}(\mathbf{X}_b)$
 $\xi_{e+1,b+1} = \mathcal{U}\left(\tau_e, \mathcal{L}\left(\hat{\mathbf{Y}}_{e,b}, \mathbf{Y}_b\right)\right)$
 end for
end for
OUTPUT: v th epoch for early stopping parameter set $\xi_{v,B}^*$

this is defined as a weight decay parameter and we set it to be 0.0005. We choose the learning rate to be constant across training, selecting $\tau^{(i)} = 7.5 \times 10^{-3}, 1 \times 10^{-3}$ (depending on model architecture), $\tau^{(a)} = 1 \times 10^{-3}$ and $\tau^{(r)} = 1 \times 10^{-3}$; all chosen empirically. In addition, we employ early stopping criteria using the validation dataset \mathcal{D}_{valid} , which retains the model with the best performance on the validation dataset across all epochs.

5.4. Results

In this section, experimental results found from solving CS-SEI, EDA, RFEC and OSR-EDA tasks on the datasets described in Section 5.1 are documented, using the experimental setup above. Across the experiments, where applicable, we display t-distributed stochastic neighbor embedding (t-SNE) plots [35] and confusion matrices, as well as quantitative metrics such as accuracy, precision, recall, F1 Score and Silhouette scores on K-Means clusters when clustering unsupervised data. The results section is structured by considering each task sequentially for different datasets. It is noted that the learnt RF fingerprints (referred to as embeddings) are typically of dimension 100 or above. However, for visualisation purposes we use t-SNE as a dimensionality reduction method in order to display the fingerprint in 2-D. Other dimensionality reduction methods such as UMAP [36] can be also used in lieu of t-SNE.

5.4.1. USE CASE 1: CS-SEI FOR DMR DATA

In this section, we document experimental work involving the DMR dataset for the CS-SEI task. Table 1 provides a summary of metrics (Accuracy, F1 Score, Precision and Recall) when evaluating trained BCNN, BILSTM, VGG19, GLFormer and FCN model architectures on the test dataset. Figures 3 and 4 display t-SNE plots and confusion matrices respectively on the test dataset. Different colours in the t-SNE plots refer to a different emitter class; notice how across all model architectures many of the emitter classes are separate with some overlap. The embeddings which are overlapped are actually the same manufacturer of DMR but different handsets, which tells us that there are crossover features for a specific model but they can still, to some degree, be separately identified by their RF fingerprints. The overlapping emitter embeddings behaviour from the t-SNE plot can also be observed in Figure 4, where confusion matrices are displayed for all the trained model architectures on this task. Emitters (2,3), (4,5) and (6,7) are unique devices but with the same make and manufacturer, and all architectures have some difficulty in fully separated their class boundaries whereas, for the most part, emitters 0 and 1 can be distinguished with better accuracy.

A Generic Machine Learning Framework for Radio Frequency Fingerprinting

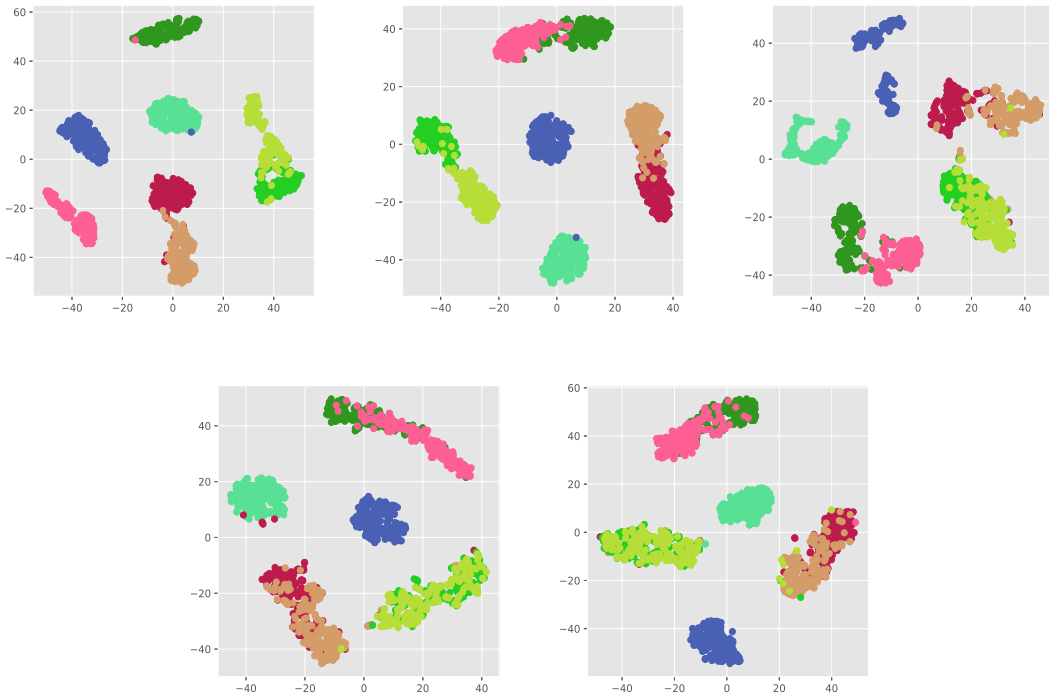


Figure 3. CS-SEI Test dataset evaluation: t-SNE data embeddings. Top: VGG19 (L), BCNN (M), GLFormer (R). Bottom: BILSTM (L), FCN (R).

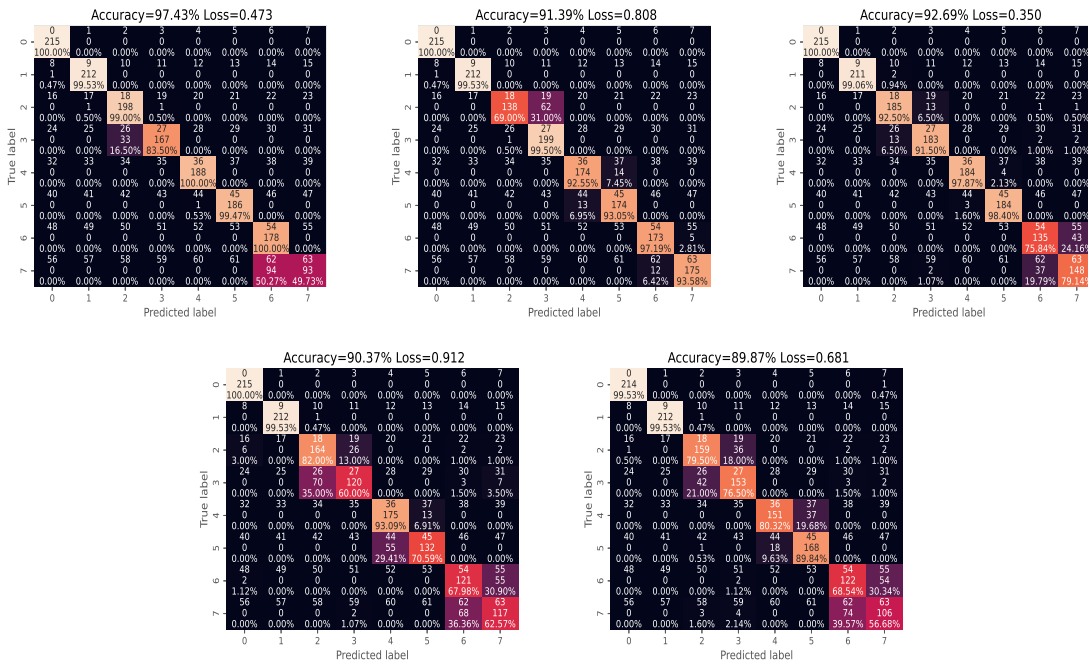


Figure 4. CS-SEI test dataset evaluation: confusion matrices. Top: VGG19 (L), BCNN (M), GLFormer (R). Bottom: BILSTM (L), FCN (R)

A Generic Machine Learning Framework for Radio Frequency Fingerprinting

Architecture	Accuracy	F1 Score	Precision	Recall
BCNN	91.68%	0.915	0.922	0.917
BILSTM	88.32%	0.881	0.906	0.884
VGG19	90.98%	0.911	0.913	0.910
GLFormer	87.30%	0.879	0.906	0.873
FCN	89.78%	0.898	0.899	0.898

Table 1. Accuracy, F1 score, precision and recall of each trained model architecture evaluated on test dataset for SEI (8 handsets)

5.4.2. USE CASE 2: CS-SEI FOR DRONE RF DATA

In this section, we document experimental results involving the RF drone dataset for the CS-SEI task. Figure 5 shows a t-SNE embeddings plot of the drone test dataset and a confusion matrix, when evaluating it with a trained FCN CS-SEI model on the RF drone dataset. Notice how the embeddings are separate with some overlap and the confusion matrix shows consistently good performance across the drone classes.

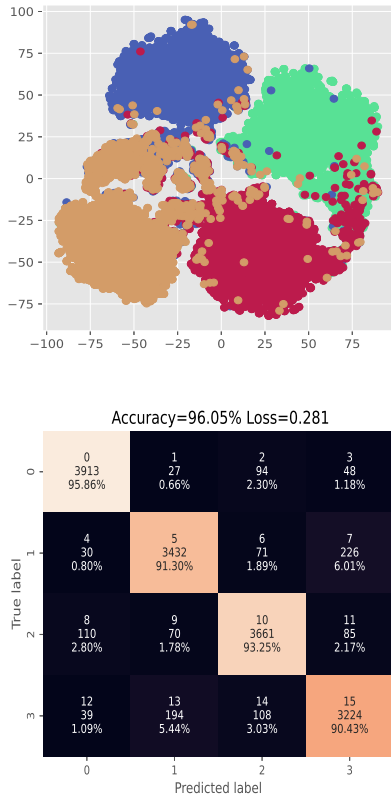


Figure 5. Drone RF links test dataset evaluation. Top: t-SNE embeddings using FCN. Bottom: confusion matrix.

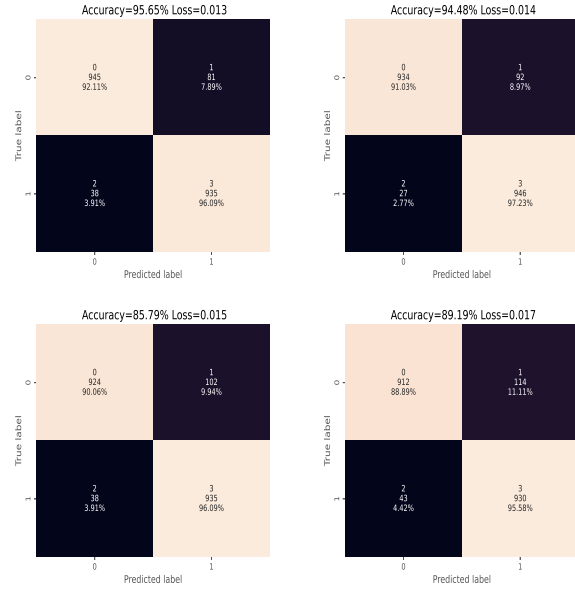


Figure 6. EDA test dataset evaluation: confusion matrices. Top: VGG19 (L), BCNN (R). Bottom: GLFormer (L), BILSTM (R).

Architecture	Accuracy	F1 Score	Precision	Recall
BCNN	94.48 %	0.940	0.910	0.972
BILSTM	89.19 %	0.921	0.889	0.955
VGG19	95.65 %	0.941	0.921	0.961
GLFormer	85.79 %	0.923	0.901	0.960

Table 2. Accuracy, F1 score, precision and recall of trained BCNN, BILSTM, VGG19, GLFormer and FCN model architectures when evaluated on the EDA test dataset.

5.4.3. USE CASE 3: EDA FOR DMR DATA

In this section, we document experimental results involving the DMR dataset for the EDA task. Figure 6 shows four confusion matrices outlining trained model performance on the EDA test dataset for four separate architectures (VGG19, BCNN, GLFormer, BILSTM). Table 2 lists the performance metrics. The results show consistent good performance and similar performance across all model architectures.

5.4.4. USE CASE 4: EDA FOR SPACEBORNE AIS DATA

Here, we present experimental results involving the AIS dataset collected by LEO satellites for the EDA task. Data from all of the 48 AIS emitters are used during the training and testing procedure, considering BCNN, BILSTM and FCN as model architectures. Figure 7 shows confusion matrices for three model architectures: BCNN, BILSTM and FCN. Similar to the other experiments, model performance is consistent across model architectures and demonstrates that ML-based RFF can deliver a high performance

A Generic Machine Learning Framework for Radio Frequency Fingerprinting

EDA, including for spaceborne maritime surveillance applications.

To assess the impact of noise on EDA performance, we synthetically add Additive White Gaussian Noise (AWGN) to the real RF captures from space, in order to generate datasets which have lower SNR. Figure 8 shows an accuracy plot of a BCNN-based EDA model against SNR. The typical trend can be seen: accuracy declines as SNR deteriorates. It is interesting to note that relying on decoding AIS burst typically requires SNRs $\gg 2dB$ whereas ML-based EDA can be accomplished at lower SNRs [61].

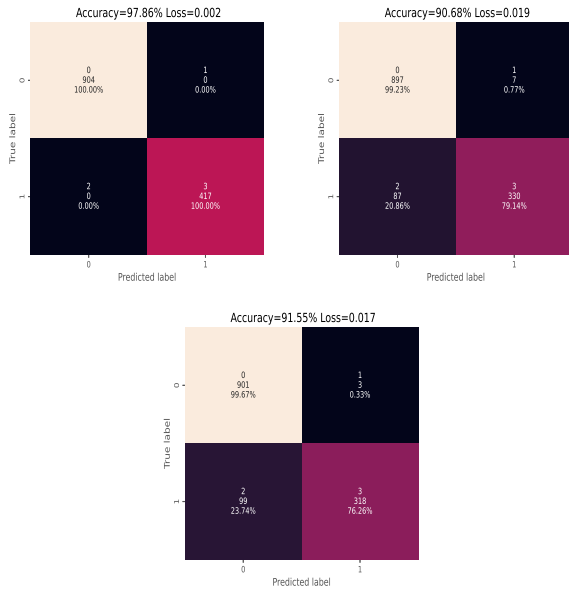


Figure 7. EDA AIS test dataset evaluation: confusion matrices. Top: BCNN (L), BILSTM (R). Bottom: FCN.

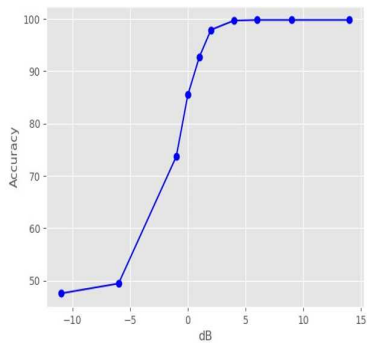


Figure 8. Accuracy vs SNR for EDA task on spaceborne AIS data.

5.4.5. USE CASE 5: RFEC FOR DMR DATA

This section presents experimental results for RFEC using the DMR dataset. Figure 9 shows t-SNE plots of the data

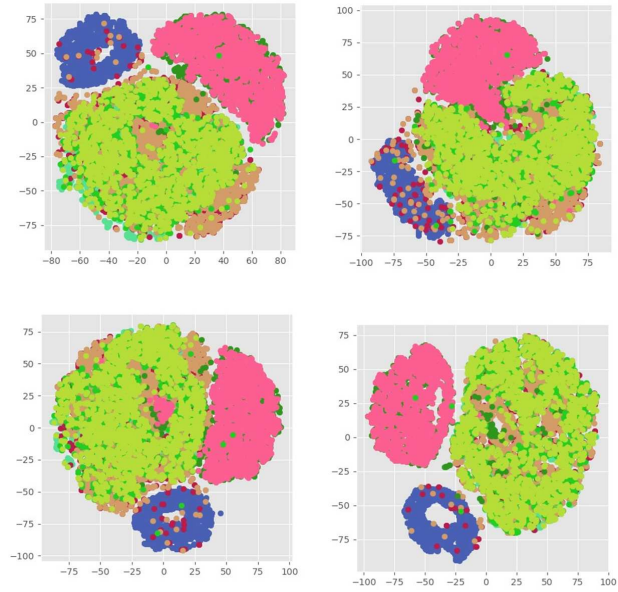


Figure 9. t-SNE plot of training dataset embeddings of DMR dataset following Emitter Representation Learning. Top: simpleAE (L), simpleconv1DAE (R). Bottom: vanillaAE (L), verysimpleAE (R).

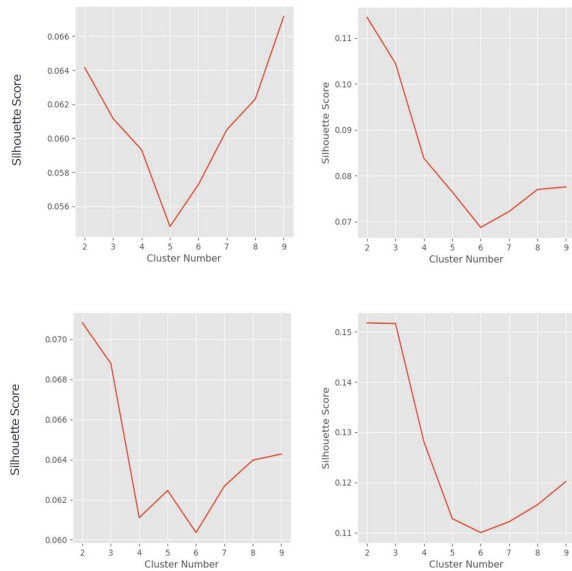


Figure 10. K-Means Silhouette scores of training dataset embeddings. Top: simpleAE (L), simpleconv1DAE (R). Bottom: vanillaAE (L), verysimpleAE (R).

embeddings for the training dataset using four model architectures. Notice how data structures have formed from learning lower dimensional representations of the emitter

A Generic Machine Learning Framework for Radio Frequency Fingerprinting

DMR via the autoencoder method. Figure 10 shows silhouette scores [46], which were computed on the training data embeddings, across a range of cluster numbers. It provides inconclusive evidence of emitters clusters being formed following unsupervised training. Nevertheless, it is included to demonstrate the RFEC task. It is possible that the DMR data has complexities which cannot be resolved via unsupervised approaches.

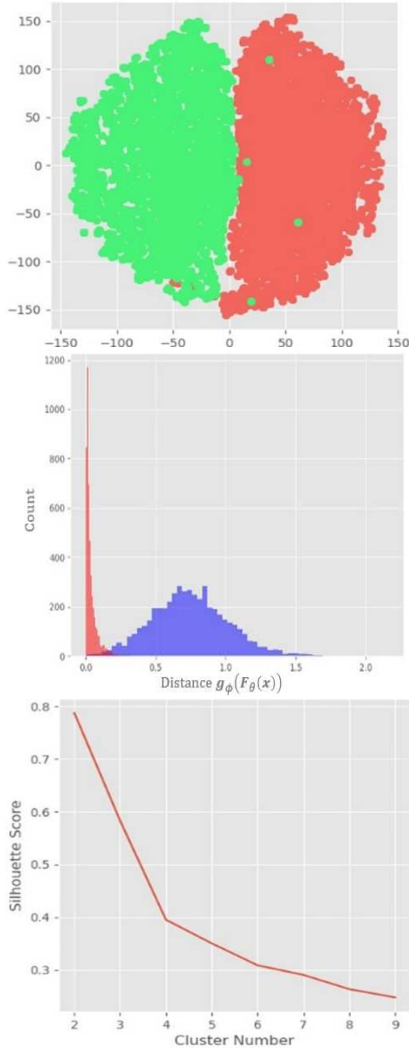


Figure 11. Held out emitter data evaluation $p = 0.5$: BCNN t-SNE embeddings (T), matched (red) and unmatched (blue) input pair distance distributions (M), K-Means Silhouette score for $K = 2, 3, \dots, 9$ (B).

5.4.6. USE CASE 6: OSR-EDA FOR DMR DATA

In this section, we present experimental results for the OSR-EDA task using the DMR dataset. Any EDA model can compare input pairs without their emitter labels, meaning we can train an EDA model on known emitters and evaluate the model on potentially unseen emitters. This is similar to

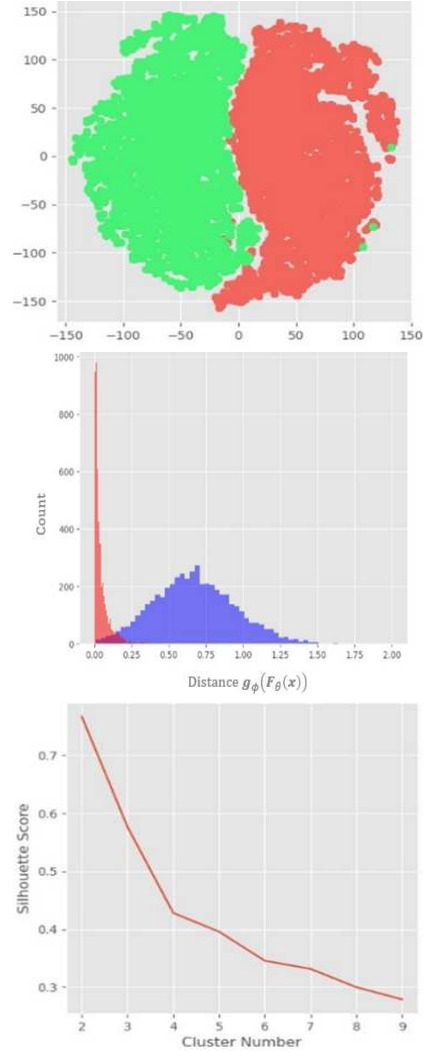


Figure 12. Held out emitter data evaluation $p = 0.25$: BCNN t-SNE embeddings (T), matched (red) and unmatched (blue) input pair distance distributions (M), K-Means Silhouette score for $K = 2, 3, \dots, 9$ (B).

the methodology in Section 4.4 but for EDA. Therefore, we trained an EDA model on the DMR dataset using emitter data from six handsets, leaving the remaining two emitters' data held out. We then evaluated the held out data using the trained EDA model to evaluate its OS capability. In addition, we adjusted a proportion parameter p of the training data to understand how much data would be needed to obtain sufficiently good performance (i.e. $p = 1$ uses all of training dataset for training, $p = 0.5$ uses half of the training dataset, etc) on the held out emitter data. Dropping data from the training dataset was done at random.

Figures 11, 12 and 13 shows a summary of the evaluation of emitter held out data using a trained EDA parameterized with a BCNN architecture for $p = 0.5, 0.25, 0.025$ respec-

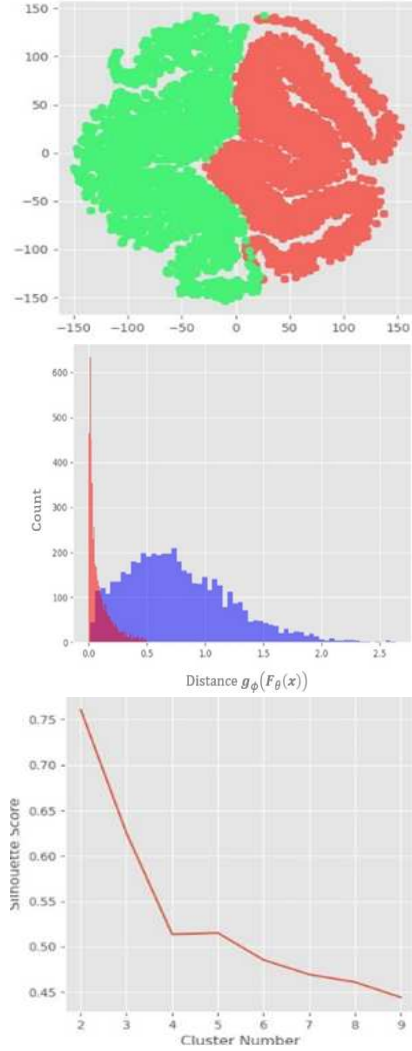


Figure 13. Held out emitter data evaluation $p = 0.025$: BCNN t-SNE embeddings (T), matched (red) and unmatched (blue) input pair distance distributions (M), K-Means Silhouette Score for $K = 2, 3, \dots, 9$ (B).

tively. Notice how the t-SNE embeddings of each emitter are distinctly separate and the distance distributions have some overlap between them but overall are quite well separated. The silhouette score is also high for cluster number 2, giving more indication on the structure of the evaluated held out emitter data. As p is reduced, however, the performance deteriorates but is minor. These are promising experimental results towards general purpose RFF models.

6. Conclusions

This paper introduces a framework for building a general-purpose machine learning RFF model. Within this, we describe a variety of RF fingerprint-related downstream tasks. We then demonstrate the four tasks SEI, EDA, RFEC and

OSR-EDA individually using three real-world RF datasets (i.e. DMR for SIGINT, AIS for maritime surveillance and drone uplink/downlink signals for C-UAS). From this, we observe that low complexity models deliver a competitive performance when compared with their more complex counterparts across all tasks and datasets. This supports the implementation of high performance data-driven RFF techniques on edge devices, which are typically characterised by a low size, weight, power and cost hardware profile. The presented generic ML-based framework for RF Fingerprinting, single task formulations, and experimental work using real RF data can stimulate future research in this domain.

A. Data Transformation Operator for EDA

Here we introduce a sampling algorithm \mathcal{M} for the EDA task. We assume that $\mathcal{D}^{(a)} = \mathcal{M}(\mathcal{D}^{(i)}) = \{(\mathbf{x}_j^{(a),1}, \mathbf{x}_j^{(a),2}, y_j^{(a)})\}_{j=1}^{n_a}$ where we choose $n_a = \gamma \ll \frac{n_i(n_i-1)}{2}$, $\gamma > 0$. Setting this condition on the number of samples in the EDA dataset is to avoid the combinatorial explosion of pairs when n_i is large. This way, we can sample from all possible pairs without completion, which could lead to a large computational overhead for some problems. For EDA labelling, we say that:

$$\tilde{y}(i, j) = \begin{cases} 1, & \text{if } y_i = y_j, \\ 0, & \text{otherwise,} \end{cases} \quad (1)$$

where $y_i, y_j \in \{1, \dots, \mathcal{V}\}$. In order to create one data-point $\mathbf{z} \in \mathcal{D}^{(a)}$, we sample twice from $\mathcal{D}^{(i)}$: $(\mathbf{x}_1, y_1) \sim \mathcal{D}^{(i)}$, $(\mathbf{x}_2, y_2) \sim \mathcal{D}^{(i)} \setminus (\mathbf{x}_1, y_1)$. Following the definition of $\tilde{y}(i, j)$, a data point $d = (x_1, x_2, \tilde{y}(1, 2))$ is created.

In general, the EDA problem has class imbalance because as the number of classes \mathcal{V} increases, the ratio of matched to unmatched pairs declines. The number of matched $n_{matched} = \mathcal{V}$ and the number of unmatched $n_{unmatched} = \frac{\mathcal{V}(\mathcal{V}-1)}{2}$. This allows us to define the ratio $n_r = \frac{n_{matched}}{n_{unmatched}} = \frac{\mathcal{V}}{\frac{1}{2}\mathcal{V}(\mathcal{V}-1)} = \frac{2}{\mathcal{V}-1}$. This can inform us on how we should structure the sampling, in terms of proportionality.

We now define a function:

$$\mathcal{C}_{ij}(\mathcal{V}; \alpha, \gamma) = \begin{cases} \frac{\alpha\gamma}{n}, & \text{if } i = j, \\ \frac{2(1-\alpha)\gamma}{n(n-1)}, & \text{if } i \neq j; \end{cases} \quad (2)$$

which determines the number of input pairs for every class pairing (i, j) , $i, j \in \{1, \dots, \mathcal{V}\}$, that is to be included in $\mathcal{D}^{(a)}$. The parameter $\alpha \in (0, 1]$ is a ratio of matched to unmatched pairs and γ is the total number of samples that is sampled from $\mathcal{D}^{(i)}$. We can structure $\mathcal{D}^{(i)}$ so that

$$\mathcal{D}^{(i)} = \{\mathcal{D}_1^{(i)}, \dots, \mathcal{D}_n^{(i)}\} \text{ where } \mathcal{D}_k^{(i)} = \{(\mathbf{x}_j^{(i)}, k)\}_{j=1}^{n_i^k} \quad (3)$$

where n_k^i is the number of samples in dataset $\mathcal{D}_k^{(i)}$. Algorithm 2 shows a recipe for computing the dataset $\mathcal{D}^{(a)}$ using $\mathcal{D}^{(i)}$.

Algorithm 2 Dataset sampling for EDA

INPUTS: proportion α , number of EDA samples γ , total number of classes \mathcal{V} , dataset $\mathcal{D}^{(i)}$

INITIALIZE: $\mathcal{D}^{(a)} = \{\}$

for $j = 1$ **to** \mathcal{V} **do**

for $k = 1$ **to** \mathcal{V} **do**

$T = \mathcal{C}_{jk}(\mathcal{V}; \alpha, \gamma)$

for $v = 1$ **to** T **do**

 Sample $d_1 = (\mathbf{x}_1, j) \sim \mathcal{D}_j^{(i)}$ and

 Sample $d_2 = (\mathbf{x}_2, k) \sim \mathcal{D}_k^{(i)} \setminus d_1$

 Set $d = (\mathbf{x}_1, \mathbf{x}_2, \tilde{y}(j, k))$

 Add d to $\mathcal{D}^{(a)}$

end for

end for

end for

OUTPUT: EDA dataset $\mathcal{D}^{(a)}$

References

- [1] Kingma DP Ba J Adam et al. A method for stochastic optimization. *arXiv preprint arXiv:1412.6980*, 1412 (6), 2014.
- [2] Jean Baptiste Alayrac, Jeff Donahue, Pauline Luc, Antoine Miech, Iain Barr, Yana Hasson, Karel Lenc, Arthur Mensch, Katherine Millican, Malcolm Reynolds, et al. Flamingo: a visual language model for few-shot learning. *Advances in neural information processing systems*, 35:23716–23736, 2022.
- [3] Aysha M Ali, Emre Uzundurukan, and Ali Kara. Assessment of features and classifiers for bluetooth rf fingerprinting. *IEEE Access*, 7:50524–50535, 2019.
- [4] Vladimir Brik, Suman Banerjee, Marco Gruteser, and Sangho Oh. Wireless device identification with radiometric signatures. In *Proceedings of the 14th ACM international conference on Mobile computing and networking*, pages 116–127, 2008.
- [5] Rich Caruana. Multitask learning. *Machine learning*, 28(1):41–75, 1997.
- [6] Guangyao Chen, Peixi Peng, Xiangqian Wang, and Yonghong Tian. Adversarial reciprocal points learning for open set recognition. *IEEE Transactions on Pattern Analysis and Machine Intelligence*, 44(11): 8065–8081, 2021.
- [7] Ting Chen, Simon Kornblith, Mohammad Norouzi, and Geoffrey Hinton. A simple framework for contrastive learning of visual representations. In *International conference on machine learning*, pages 1597–1607. PmLR, 2020.
- [8] Boris Danev and Srdjan Capkun. Transient-based identification of wireless sensor nodes. In *2009 International Conference on Information Processing in Sensor Networks*, pages 25–36. IEEE, 2009.
- [9] Boris Danev, Thomas S Heydt-Benjamin, Srdjan Capkun, et al. Physical-layer identification of rfid devices. In *USENIX security symposium*, pages 199–214, 2009.
- [10] Pengfei Deng, Shaohua Hong, Jie Qi, Lin Wang, and Haixin Sun. A lightweight transformer-based approach of specific emitter identification for the automatic identification system. *IEEE Transactions on Information Forensics and Security*, 18:2303–2317, 2023.
- [11] Lida Ding, Shilian Wang, Fanggang Wang, and Wei Zhang. Specific emitter identification via convolutional neural networks. *IEEE communications letters*, 22(12):2591–2594, 2018.
- [12] Martin Ester, Hans-Peter Kriegel, Jörg Sander, Xiaowei Xu, et al. A density-based algorithm for discovering clusters in large spatial databases with noise. In *kdd*, volume 96, pages 226–231, 1996.
- [13] Martins Ezuma, Fatih Erden, Chethan Kumar Anjinnappa, Ozgur Ozdemir, and Ismail Guvenc. Micro-uav detection and classification from rf fingerprints using machine learning techniques. In *2019 IEEE Aerospace Conference*, pages 1–13. IEEE, 2019.
- [14] Henrik Forssell, Evgeny Kharlamov, and Evgenij Thorstensen. On equivalence and cores for incomplete databases in open and closed worlds. *arXiv preprint arXiv:2001.04757*, 2020.
- [15] Hua Fu, Linning Peng, Ming Liu, and Aiqun Hu. Deep learning-based rf fingerprint identification with channel effects mitigation. *IEEE Open Journal of the Communications Society*, 4:1668–1681, 2023.
- [16] Alex Graves, Abdel-rahman Mohamed, and Geoffrey Hinton. Speech recognition with deep recurrent neural networks. In *2013 IEEE international conference on acoustics, speech and signal processing*, pages 6645–6649. Ieee, 2013.
- [17] Samer Hanna, Samurdhi Karunaratne, and Danijela Cabric. Wisig: A large-scale wifi signal dataset for receiver and channel agnostic rf fingerprinting. *IEEE Access*, 10:22808–22818, 2022.

- [18] Sepp Hochreiter and Jürgen Schmidhuber. Long short-term memory. *Neural computation*, 9(8):1735–1780, 1997.
- [19] Yuanling Huang et al. Radio frequency fingerprint extraction of radio emitter based on i/q imbalance. *Procedia computer science*, 107:472–477, 2017.
- [20] Sergey Ioffe and Christian Szegedy. Batch normalization: Accelerating deep network training by reducing internal covariate shift. In *International conference on machine learning*, pages 448–456. pmlr, 2015.
- [21] Anu Jagannath, Jithin Jagannath, and Prem Sagar Pattanshetty Vasanth Kumar. A comprehensive survey on radio frequency (rf) fingerprinting: Traditional approaches, deep learning, and open challenges. *Computer Networks*, 219:109455, 2022.
- [22] Tong Jian, Bruno Costa Rendon, Emmanuel Ojuba, Nasim Soltani, Zifeng Wang, Kunal Sankhe, Andrey Gritsenko, Jennifer Dy, Kaushik Chowdhury, and Stratis Ioannidis. Deep learning for rf fingerprinting: A massive experimental study. *IEEE Internet of Things Magazine*, 3(1):50–57, 2020.
- [23] Qi Jiang and Jin Sha. Radio frequency fingerprint identification based on variational autoencoder for gnss. *IEEE Geoscience and Remote Sensing Letters*, 21:1–4, 2024.
- [24] SeyedMohammad Kashani, Syed Mujtaba Sherazi, Ashfaq Khokhar, Sang Wu Kim, and Farid Nait-Abdesselam. Radio frequency fingerprinting in wbans using complex-valued convolutional neural networks. In *2024 International Wireless Communications and Mobile Computing (IWCMC)*, pages 1631–1636. IEEE, 2024.
- [25] Irwin O Kennedy, Patricia Scanlon, Francis J Mullany, Milind M Buddhikot, Keith E Nolan, and Thomas W Rondeau. Radio transmitter fingerprinting: A steady state frequency domain approach. In *2008 IEEE 68th Vehicular Technology Conference*, pages 1–5. IEEE, 2008.
- [26] Yann LeCun, Léon Bottou, Yoshua Bengio, and Patrick Haffner. Gradient-based learning applied to document recognition. *Proceedings of the IEEE*, 86(11):2278–2324, 2002.
- [27] Dingzhao Li, Jie Qi, Shaohua Hong, Pengfei Deng, and Haixin Sun. A class-incremental approach with self-training and prototype augmentation for specific emitter identification. *IEEE Transactions on Information Forensics and Security*, 19:1714–1727, 2023.
- [28] Dingzhao Li, Xiaowei Chen, Shaohua Hong, Jie Qi, and Haixin Sun. Fscil-sei: Few-shot class-incremental learning approach for specific emitter identification. *IEEE Transactions on Instrumentation and Measurement*, 2025.
- [29] Dingzhao Li, Zhendong Chen, Mingyuan Shao, Xiaowei Chen, Shaohua Hong, Jie Qi, and Haixin Sun. Non-exemplar class-incremental learning via prototype correction and hierarchical regularization for specific emitter identification. *IEEE Transactions on Intelligent Transportation Systems*, 2025.
- [30] Zhizhong Li and Derek Hoiem. Learning without forgetting. *IEEE transactions on pattern analysis and machine intelligence*, 40(12):2935–2947, 2017.
- [31] Min Lin, Qiang Chen, and Shuicheng Yan. Network in network. *arXiv preprint arXiv:1312.4400*, 2013.
- [32] Mingqian Liu, Jiakun Wang, and Cheng Qian. Incremental learning based radio frequency fingerprint identification using intelligent representation. In *IEEE INFOCOM 2021-IEEE Conference on Computer Communications Workshops (INFOCOM WKSHPS)*, pages 1–6. IEEE, 2021.
- [33] Yuanyuan Lv, Yuanan Liu, Fang Liu, Jinchun Gao, Kaiming Liu, and Gang Xie. Automatic modulation recognition of digital signals using cwt based on optimal scales. In *2014 IEEE International Conference on Computer and Information Technology*, pages 430–434. IEEE, 2014.
- [34] Andrew L Maas, Awni Y Hannun, Andrew Y Ng, et al. Rectifier nonlinearities improve neural network acoustic models. In *Proc. icml*, volume 30, page 3. Atlanta, GA, 2013.
- [35] Laurens van der Maaten and Geoffrey Hinton. Visualizing data using t-sne. *Journal of machine learning research*, 9(Nov):2579–2605, 2008.
- [36] Leland McInnes, John Healy, and James Melville. Umap: Uniform manifold approximation and projection for dimension reduction. *arXiv preprint arXiv:1802.03426*, 2018.
- [37] Rui Meng, Bingxuan Xu, Xiaodong Xu, Mengying Sun, Bizhu Wang, Shujun Han, Suyu Lv, and Ping Zhang. A survey of machine learning-based physical-layer authentication in wireless communications. *Journal of network and computer applications*, 235:104085, 2025.

- [38] Kevin Merchant and Bryan Nousain. Enhanced rf fingerprinting for iot devices with recurrent neural networks. In *MILCOM 2019-2019 IEEE Military Communications Conference (MILCOM)*, pages 590–597. IEEE, 2019.
- [39] Kevin Merchant and Bryan Nousain. Securing iot rf fingerprinting systems with generative adversarial networks. In *MILCOM 2019-2019 IEEE Military Communications Conference (MILCOM)*, pages 584–589. IEEE, 2019.
- [40] Xuran Pan, Tianzhu Ye, Zhuofan Xia, Shiji Song, and Gao Huang. Slide-transformer: Hierarchical vision transformer with local self-attention. In *Proceedings of the IEEE/CVF conference on computer vision and pattern recognition*, pages 2082–2091, 2023.
- [41] Can Peng, Kun Zhao, Tianren Wang, Meng Li, and Brian C Lovell. Few-shot class-incremental learning from an open-set perspective. In *European Conference on Computer Vision*, pages 382–397. Springer, 2022.
- [42] Linning Peng, Junqing Zhang, Ming Liu, and Aiqun Hu. Deep learning based rf fingerprint identification using differential constellation trace figure. *IEEE Transactions on Vehicular Technology*, 69(1):1091–1095, 2019.
- [43] Alec Radford, Jong Wook Kim, Chris Hallacy, Aditya Ramesh, Gabriel Goh, Sandhini Agarwal, Girish Sastry, Amanda Askell, Pamela Mishkin, Jack Clark, et al. Learning transferable visual models from natural language supervision. In *International conference on machine learning*, pages 8748–8763. PmLR, 2021.
- [44] Xubin Ren, Wei Wei, Lianghao Xia, and Chao Huang. A comprehensive survey on self-supervised learning for recommendation. *ACM Computing Surveys*, 58(1):1–38, 2025.
- [45] Josh Robinson, Scott Kuzdeba, James Stankowicz, and Joseph M Carmack. Dilated causal convolutional model for rf fingerprinting. In *2020 10th Annual Computing and Communication Workshop and Conference (CCWC)*, pages 0157–0162. IEEE, 2020.
- [46] Peter J Rousseeuw. Silhouettes: a graphical aid to the interpretation and validation of cluster analysis. *Journal of computational and applied mathematics*, 20: 53–65, 1987.
- [47] Kunal Sankhe, Mauro Belgiovine, Fan Zhou, Shamnaz Riyaz, Stratis Ioannidis, and Kaushik Chowdhury. Oracle: Optimized radio classification through convolutional neural networks. In *IEEE INFOCOM 2019-IEEE conference on computer communications*, pages 370–378. IEEE, 2019.
- [48] Walter J Scheirer, Anderson de Rezende Rocha, Archana Sapkota, and Terrance E Boulton. Toward open set recognition. *IEEE transactions on pattern analysis and machine intelligence*, 35(7):1757–1772, 2012.
- [49] Ozan Sener and Vladlen Koltun. Multi-task learning as multi-objective optimization. *Advances in neural information processing systems*, 31, 2018.
- [50] Guanxiong Shen, Junqing Zhang, Alan Marshall, Lining Peng, and Xianbin Wang. Radio frequency fingerprint identification for lora using deep learning. *IEEE Journal on Selected Areas in Communications*, 39(8):2604–2616, 2021.
- [51] Guanxiong Shen, Junqing Zhang, Alan Marshall, and Joseph R Cavallaro. Towards scalable and channel-robust radio frequency fingerprint identification for lora. *IEEE Transactions on Information Forensics and Security*, 17:774–787, 2022.
- [52] Karen Simonyan and Andrew Zisserman. Very deep convolutional networks for large-scale image recognition. *arXiv preprint arXiv:1409.1556*, 2014.
- [53] Joshua Smailes, Sebastian Köhler, Simon Bimbach, Martin Strohmeier, and Ivan Martinovic. Satiq: Extensible and stable satellite authentication using hardware fingerprinting. *ACM Transactions on Privacy and Security*, 2025.
- [54] Naeimeh Soltanieh, Yaser Norouzi, Yang Yang, and Nemaï Chandra Karmakar. A review of radio frequency fingerprinting techniques. *IEEE Journal of Radio Frequency Identification*, 4(3):222–233, 2020.
- [55] Ashish Vaswani, Noam Shazeer, Niki Parmar, Jakob Uszkoreit, Llion Jones, Aidan N Gomez, Łukasz Kaiser, and Illia Polosukhin. Attention is all you need. *Advances in neural information processing systems*, 30, 2017.
- [56] Sagar Vaze, Kai Han, Andrea Vedaldi, and Andrew Zisserman. Open-set recognition: A good closed-set classifier is all you need? *arXiv:2110.06207*, 2021.
- [57] Wenhui Wang, Hangbo Bao, Li Dong, Johan Bjorck, Zhiliang Peng, Qiang Liu, Kriti Aggarwal, Owais Khan Mohammed, Saksham Singhal, Subhojit Som, et al. Image as a foreign language: Beit pre-training for vision and vision-language tasks. In *Proceedings of the IEEE/CVF Conference on Computer Vision and Pattern Recognition*, pages 19175–19186, 2023.

A Generic Machine Learning Framework for Radio Frequency Fingerprinting

- [58] Xueli Wang, Yufeng Zhang, Hongxin Zhang, Yixuan Li, and Xiaofeng Wei. Radio frequency signal identification using transfer learning based on lstm. *Circuits, Systems, and Signal Processing*, 39(11):5514–5528, 2020.
- [59] Yu Wang, Guan Gui, Yun Lin, Hsiao-Chun Wu, Chau Yuen, and Fumiyuki Adachi. Few-shot specific emitter identification via deep metric ensemble learning. *IEEE Internet of Things Journal*, 9(24):24980–24994, 2022.
- [60] Yu Wang, Tomoaki Ohtsuki, Zhi Sun, Dusit Niyato, Xianbin Wang, and Guan Gui. Avoiding shortcuts: Enhancing channel-robust specific emitter identification via single-source domain generalization. *IEEE Transactions on Wireless Communications*, 2025.
- [61] Roman Wawrzaszek, Marcin Waraksa, Maciej Kalarus, Grzegorz Juchnikowski, and Tomasz Górski. Detection and decoding of ais navigation messages by a low earth orbit satellite. In *Aerospace Robotics III*, pages 45–62. Springer, 2018.
- [62] Qingyang Wu, Carlos Feres, Daniel Kuzmenko, Ding Zhi, Zhou Yu, Xin Liu, and Xiaoguang ‘Leo’Liu. Deep learning based rf fingerprinting for device identification and wireless security. *Electronics Letters*, 54(24):1405–1407, 2018.
- [63] Feiyi Xie, Hong Wen, Yushan Li, Songlin Chen, Lin Hu, Yi Chen, and Huanhuan Song. Optimized coherent integration-based radio frequency fingerprinting in internet of things. *IEEE Internet of Things Journal*, 5(5):3967–3977, 2018.
- [64] Wei Xie, Hongjun Wang, Zhexian Shen, Xinhao Li, Zhiquan Liu, and Hao Jiang. A novel radio frequency fingerprint identification scheme for few-shot open-set recognition. *IEEE Internet of Things Journal*, 2025.
- [65] Ning Yang, Bangning Zhang, Guoru Ding, Yimin Wei, Guofeng Wei, Jian Wang, and Daoxing Guo. Specific emitter identification with limited samples: A model-agnostic meta-learning approach. *IEEE Communications Letters*, 26(2):345–349, 2021.
- [66] Jiabao Yu, Aiqun Hu, Guyue Li, and Linning Peng. A robust rf fingerprinting approach using multisampling convolutional neural network. *IEEE internet of things journal*, 6(4):6786–6799, 2019.
- [67] Jiabao Yu, Aiqun Hu, Fen Zhou, Yuexiu Xing, Yi Yu, Guyue Li, and Linning Peng. Radio frequency fingerprint identification based on denoising autoencoders. In *2019 International Conference on Wireless and Mobile Computing, Networking and Communications (WiMob)*, pages 1–6. IEEE, 2019.
- [68] Ying Zhang, Qiang Li, Hongli Liu, Liu Yang, and Jian Yang. Domain generalization for cross-receiver radio frequency fingerprint identification. *IEEE Internet of Things Journal*, 2024.
- [69] Yu Zhang and Qiang Yang. A survey on multi-task learning. *IEEE transactions on knowledge and data engineering*, 34(12):5586–5609, 2021.
- [70] Yuanyu Zhang, Jia’Ning Wang, Zhumeng Zheng, Yulong Shen, Yunsong Jiang, and Mengfei Yang. Variational autoencoder-based radio frequency fingerprinting for gps anti-spoofing. In *2024 International Conference on Networking and Network Applications (NaNA)*, pages 172–178. IEEE, 2024.
- [71] Fei Zhu, Zhen Cheng, Xu-Yao Zhang, and Cheng-lin Liu. Class-incremental learning via dual augmentation. *Advances in neural information processing systems*, 34:14306–14318, 2021.